CONF-830911--33

UCRL- 89881
PREPRINT

UCRL--89881

DE84 001421

BEAM DYNAMICS IN THE ADVANCED TEST ACCELERATOR (ATA)

G. J. Caporaso, W. A. Barletta, D. L. Birx
R. J. Briggs, Y. P. Chong, A. G. Cole,
T. J. Fessenden, R. E. Hester, E. J. Lauer,
V. K. Neil, A. C. Paul, D. S. Prono and
K. W. Struve

This paper was prepared for presentation at
the Fifth International Conference on
High-Power Particle Beams
San Francisco, CA
September 12 - 14, 1983

September 28, 1983

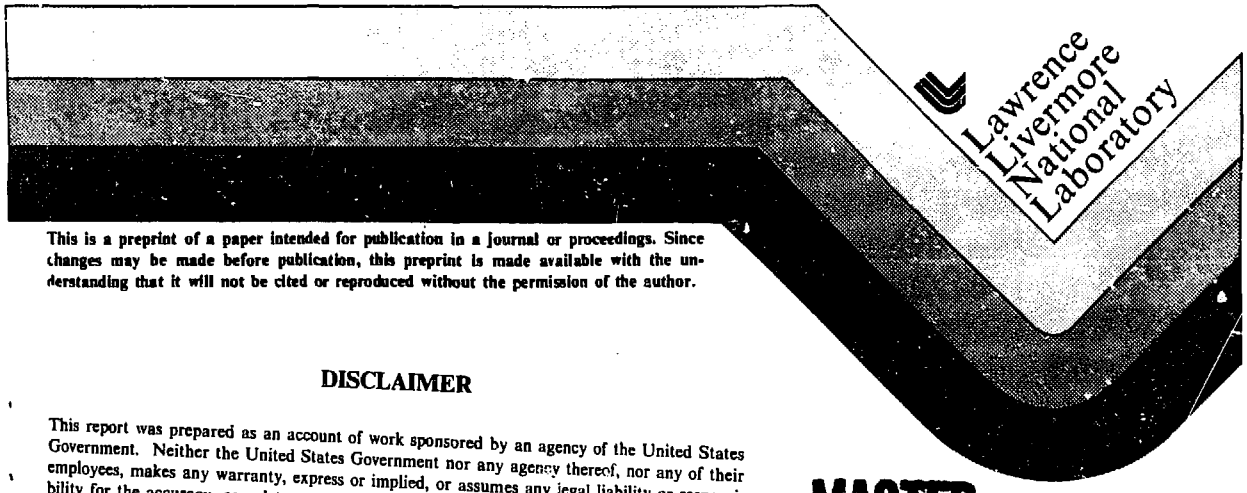

DISCLAIMER

BEAM DYNAMICS IN THE ADVANCED TEST ACCELERATOR (ATA)*

G. J. Caporaso, W. A. Barletta, D. L. Birx,
R. J. Briggs, Y. P. Chong, A. G. Cole, T. J. Fessenden,
R. E. Hester, E. J. Lauer, V. K. Neil, A. C. Paul,
D. S. Prono and K. W. Struve

Lawrence Livermore National Laboratory
University of California
P.O. Box 808
Livermore, CA 94550

Abstract

We will review the performance of the Advanced Test Accelerator, a 50 MeV, 10 KA induction linac. The discussion will cover the operation of the plasma cathode electron source, beam transport throughout the accelerator, and transverse instabilities. Particular emphasis will be placed on the beam breakup instability and on the methods used to minimize it. These include a program of design changes that lead to an order of magnitude reduction in the Q's of the accelerator cavity modes and optimization of the transport tune.

Introduction and Summary of Performance

The Advanced Test Accelerator (ATA) is a 50 MeV, 10 KA, 70 nsec. pulse width electron linear induction accelerator consisting of 170 accelerating cavities and a 2.5 MeV injector. The injector has achieved its design goal of generating a 10 KA, 2.5 MeV beam. Thus far 10 KA has been accelerated to 15 MeV and 1.5 KA has been accelerated to 50 MeV. The beam breakup (BBU) instability has been observed and is under active investigation.

Initial Operation

Initial operation of ATA concentrated on characterization of the injector and a study of beam dynamics up to the 10 MeV point in the accelerator. A diagram of the beamline is shown in Fig. 1. The electron source is a surface discharge plasma cathode shown in Fig. 2 [1]. A sketch of the cathode illustrating its mode of operation is shown in Fig. 3. Sixteen hundred double rings are etched onto the surface of a printed circuit board that constitutes a ground plane. A high voltage pulse is applied through a resistor to the center pad of each double ring. A discharge across the double ring then developes which desorbs and ionizes some adsorbed gas. The beam current is then extracted from the plasma by applying a potential to a nearby

*Performed jointly under the auspices of the U.S. DOE by LLNL under W-7405-ENG-48 and for the DOD under DARPA, ARPA order No. 4395, monitored by NSWC.

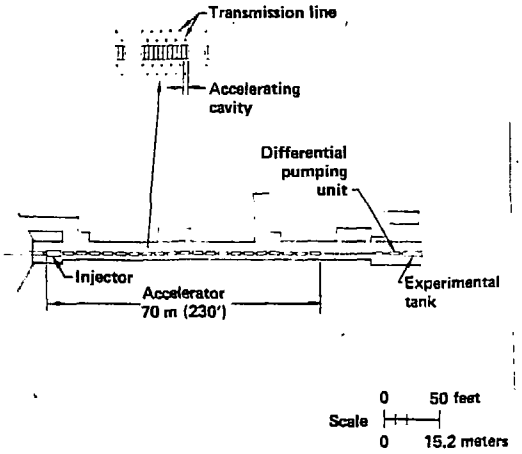

Fig. 1. Schematic of the ATA showing the 2.5 MeV injector and 20 accelerating blocks. The first 6 blocks contain 5 cavities each while the remaining 14 contain 10 cavities each.

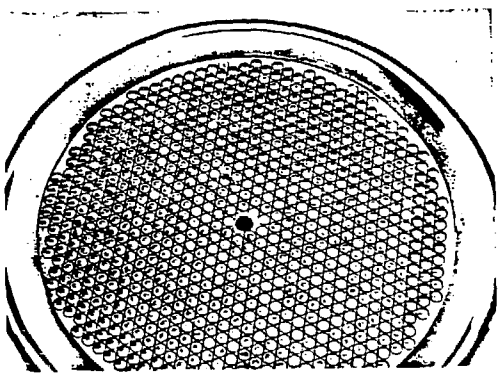

Fig.2. Photo of an older type plasma cathode. The active region (containing the rings) is 10 inches in diameter.

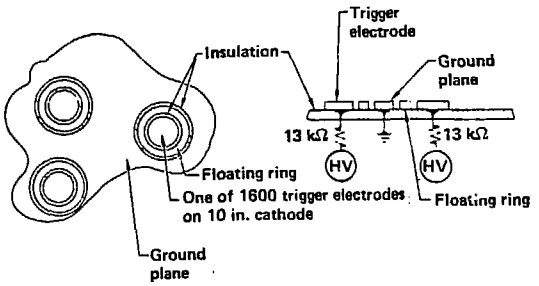

Fig. 3. Drawing of the ATA cathode. A high voltage pulse applied to the center of each double ring initiates a discharge to ground desorbing and ionizing surface gases from which the beam is extracted.

grid. The measured emittance is close to the anticipated value and is shown in Fig. 4.

The accelerator beamline is instrumented with resistive wall current monitors [2] which measures beam current and X and Y components of the beam centroid as functions of time, and also with RF loops which measure the time derivative of B_θ produced by the beam [3]. In addition there are ports for x-ray dot probes which are used to determine beam profiles.

Data from the initial operation of ATA revealed several undesirable features which are evident in Figs. 5 and 6. Figure 5a shows the beam current and X and Y positions just downstream of the injector while Fig. 5b shows the corresponding data at the 10 MeV point. The deterioration of the beam centroid offset is obvious. Figure 6a shows a typical "quiet" RF loop signal at the injector output while Fig. 6b shows the worst (largest) BBU signal seen to date at the 10 MeV point. The 800 MHz. signal in the body of the pulse is the beam breakup instability and is of substantially larger amplitude than that expected on the basis of previous injector noise measurements [3]. Also visible on the head of the RF loop signal in 6b is a lower frequency "hash" of several millimeters in amplitude.

Subsequent installation of collimating apertures in the beamline and modification of the injector operating conditions have substantially affected the beam transport, and at least one of the troublesome mechanisms is now understood.

Beam Breakup (BBU) Instability

This transverse instability arises from the beam excitation of the dipole (m=1) transverse magnetic modes of the accelerator cavities[4]. BBU

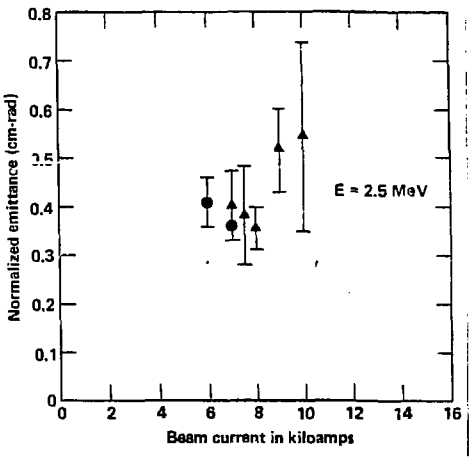

Fig. 4. Normalized emittance vs. beam current determined from injector measurements.

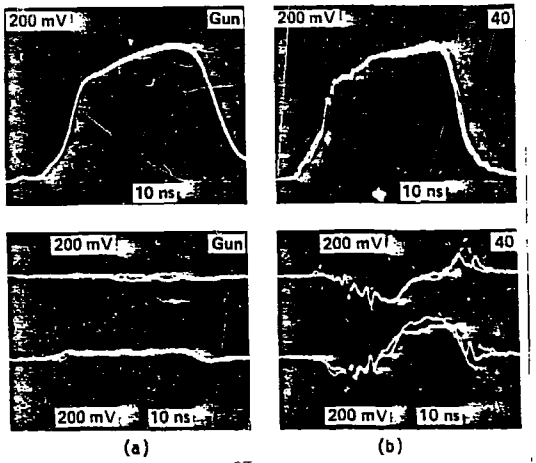

Fig. 5. Current and current weighted X and Y displacements (a) (left) out of injector and (b) (right) at the 10 MeV point.

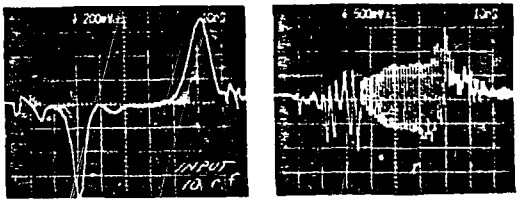

Fig. 6. (a) typical RF (B_θ) loop signal at injector output. (b) worst (largest) BBU signal observed thus far (800 MHZ oscillations in the pulse body). Transverse displacement for BBU =1 mm.

has been extensively studied on the 8 cavity Experimental Test Accelerator (ETA). Modifications were made to the cavities in order to reduce the Q's of the transverse modes. This was accomplished by inserting pieces of ferrite at several locations as shown in Fig. 7. Also installed was a reflector to permit better matching of radially propagating waves around the corner of the cavity and into the damping ferrite. The Q of the ATA cavities was reduced from 40 to about 4 [5].

The transverse shunt impedance of the cavities, $Z_\perp/Q$, was measured dynamically on ETA by using a beam excited tickler cavity to inject a BBU signal into the accelerator and measuring the resulting BBU gain [3]. Our best determination for the ATA cavity $Z_\perp/Q$ is = 6.9 ohms.

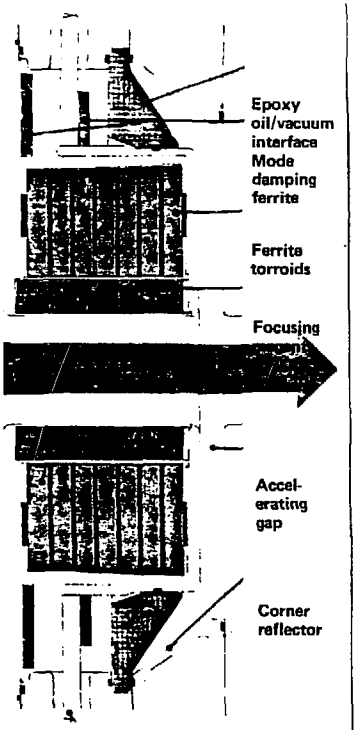

Fig. 7. ATA cavity showing modifications made to reduce Q's of the TM_{1n0} modes. Shown is the corner reflector which permits the modes to penetrate the interface and reach the mode damping ferrites.

The dominant mode has a frequency of 785 MHz. Under these conditions analytic and code results predict a BBU growth through the entire ATA of roughly 10^4 at a beam current of 10 KA. Early noise measurements of the ATA injector yielded 785 MHZ amplitudes of $\sim 1.8 \times 10^{-4}$ cm leading to expectations of centimeter size transverse displacements at the end of ATA. The dependence of BBU growth on the relevant parameters is made explicit by the asymptotic formula,

$$\xi \propto \xi_0 \exp\left[\frac{1.16 \times 10^{-13} N\omega Q\,(Z_\perp/Q) I_{KA}}{B_{kg}}\right] \qquad (1)$$

where N is the number of cavities, I is the beam current in KA, ω is the angular frequency of the mode and B is the average solenoidal field in kilogauss.

Results of the initial 10 MeV ATA runs shown in Fig. 6 reveal a BBU amplitude some 30 times greater than anticipated. However, additional RF loops placed upstream revealed that the growth of the BBU as a function of distance was as expected pointing towards an excitation level 30 times larger than has been previously measured. As will be shown subsequently changing the injector operating conditions and collimating the beam at the output of the injector dramatically reduced the BBU amplitude.

"Corkscrew" Mode

One feature of the RF loop waveforms in Fig. 6b can be understood in terms of a simple model. Consider a beam having a variation of energy over its length which is uniformly transversely displaced. As the beam propagates in a solenoidal field various portions of it will rotate through different angles because each portion has a different γ. After enough cyclotron turns the beam, which was originally uniformly offset, will resemble a corkscrew.

For example if $X = 2X_0$, $\partial Y/\partial Z = KX_0$, and $Y = \partial Y/\partial Z = 0$ at $Z = 0$ then for $Z > 0$, $X(Z) = X_0\,(1+\cos(KZ))$ and $Y(Z) = X_0 \sin(KZ)$. Now if we take $\gamma = \gamma_0 \times (1 + \frac{\Delta\gamma}{\gamma_0} \sin\omega t)$ so that $K = K_0/(1 + \frac{\Delta\gamma}{\gamma_0} \sin\omega t)$ and consider $Y(Z,t)$ only, we have

$$Y(Z,t) = X_0 \sin\left[\frac{K_0 Z}{1 + \frac{\Delta\gamma}{\gamma_0} \sin\omega t}\right] . \qquad (2)$$

If $K_0 Z (\frac{\Delta\gamma}{\gamma_0})^2 \ll 1$ we may approximate $Y(Z,t)$ as

$$Y(Z,t) = X_0 \sin\left[K_0 Z \left\{1 - \frac{\Delta\gamma}{\gamma_0} \sin\omega t\right\}\right] . \qquad (3)$$

Using the expansions $COS(XSIN\theta) = J_0(X) + 2 \times [J_2(X)COS2\theta + J_4(X)COS4\theta + \ldots]$ and $SIN(XSIN\theta) = 2[J_1(X)SIN\theta + J_3(X)SIN3\theta + \ldots]$ we see that the amplitude of the nth harmonic of ω is

$$a_n = 2 X_0 J_n(K_0 Z \frac{\Delta\gamma}{\gamma_0}) \cong 2X_0 \left(\frac{K_0 Z \Delta\gamma}{2\gamma_0}\right)^n \quad . \quad (4)$$

Thus the original uniform offset gives rise to a time varying displacement whose frequency upshifts with Z eventually attaining the amplitude of the original offset. This is important for BBU since the frequency will eventually upshift enough to excite the mode even if the injector noise at 800 MHZ is small.

In the ATA the source of the gamma variation is the beam loading of the accelerator cavities which leads to variations of γ on the head and tail of the pulse as is seen in Fig. 8. When this gamma variation is folded together with the observed offsets in simulations good agreement with the RF loop data is obtained. However, the original source of the beam offset is not accounted for by this picture.

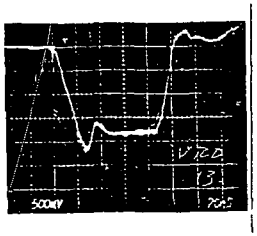

Fig. 8. Typical signal proportional to cavity accelerating voltage showing the loading of the drive by the beam current. The voltage change is largest at the head and tail of the pulse.

"Notching"

Examination of Fig. 5 reveals several other interesting features. First the beam offsets which are fairly small at the injector output have grown downstream. Secondly the rising and falling edges of the downstream current signals have notches. The interpretation of the notches is not yet clear. At least some of the signals can probably be explained as arising from current loss on the walls. Some of the data indicates possible bunching. In addition, there is a small degree of current loss as the beam propagates down the machine that is evident from regularly spaced wall current monitors.

Collimation Experiments

Initial x-ray profile measurements indicated that the beam was non-uniform as it emerged from the injector. For this reason a set of 3 collimating apertures 6 cm in diameter spaced approximately 50 cm apart was placed in the beamline just downstream of the injector. Although only 5 to 10% of the beam current was lost on the apertures there was a significant decrease in beam offset downstream.

The apertures were replaced with ones that were 4 cm in diameter and some further improvement was noted. At this point injector operating condition sensitivety tests were performed and the operating length of the accelerator was extended through 20 additional cavities to the 15 MeV point.

Injector Operating Condition Experiments

The basic variables adjusted in this series of experiments were the igniter to grid timing and the grid to anode timing. In normal operation the igniter pulse which creates the cathode plasma is applied some 60 nsec. prior to the grid pulse. This permits the cathode plasma to advance a significant distance towards the grid before beam current is extracted. The anode pulse is applied before the grid pulse so that the extracted beam will have a relatively constant energy.

An experiment was performed in which the igniter timing was delayed by approximately 40-48 nsec. so that the grid pulse was applied only 12 to 20 nsec. after the igniter pulse. There was a dramatic reduction in the BBU levels measured downstream. Figure 9a shows the downstream current, X, Y and RF loop signals at the 10 MeV point with normal timing while the corresponding signals for delayed timing are shown in Fig. 9b.

Normally the cathode is shielded from the solenoidal field by two bucking coils. An interesting series of experiments was done in which one of the coils was reversed permitting some B_z to thread the cathode. the resulting field was so large (~100 gauss) that the beam was no longer space charge dominated and the beam radius upon entrance to the aperture set was increased resulting in lower current transmission through the apertures. This resulted in less beam offset downstream and in less sweep, or variation of the offset throughout the pulse. The comparison is shown in Fig. 10. An experiment was performed to see if coherent beam-cavity interactions, which presumably depend on current, were contributing significantly to notching or to the development of beam offsets. The magnetic field in the vicinity of the apertures was greatly weakened permitting all but about 500A to be lost on the apertures. The notching, offsets and sweep were found to be qualitatively similar for the two cases.

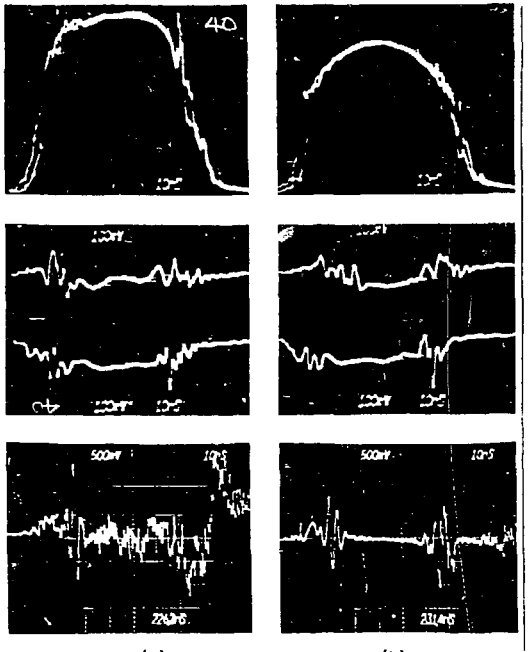

(a) (b)

Fig. 9. Current, current weighted X and Y offsets and RF loop signals at the 10 MeV point for (a) normal injector timing and (b) delayed injector timing. Note the disappearence of the BBU.

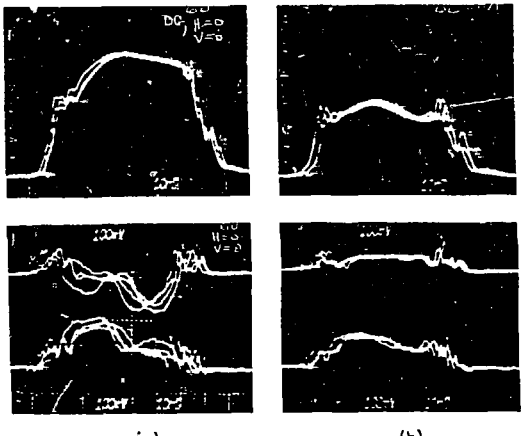

(a) (b)

Fig. 10. Current and current weighted X and Y offsets at the 10 MeV point for (a) normal bucking coil operation and (b) reversed bucking coil operation. Note the reduced sweep in (b).

An x-ray dot probe was used to look at the beam profile at the 10 MeV point under conditions of normal injector timing and a beam current of 5KA. The raw data and reduced data are shown in Fig. 11. The current profile is quite broad.

Much of the experimental evidence collected to date indicates that the injector is generating a non-uniform noisy beam which proper collimation should improve.

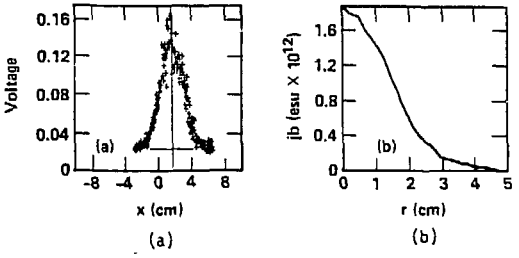

Fig. 11. Beam profile as determined from x-ray probe measurements at 10 MeV point during the peak of the pulse (a) raw data and (b) average current density vs. radius.

Present Status

The collimating apertures are being replaced with a continuous 110 cm long 4 cm diameter pipe which should provide more reliable collimation than three separate apertures. The operating beamline will be extended from the 15 MeV point through 20 additional cells to the 20 MeV point for further experimentation before operation of the entire accelerator. In addition a wire zone will be installed at the 6.0 MeV point to damp out beam offsets and sweep and to symmetrize the beam. This experiment will serve to decouple the injector from the accelerator, providing information on the degree to which the observed beam problems are due to some aspect of the source.

Wire Zone

An electrostatically charged wire has been routinely used to strongly guide, focus and damp up to 8KA beams at the output of ETA [6]. A sketch of the system is shown in Fig. 12. A highly resistive, conducting wire is stretched out between two conducting end foils. In the presence of a beam the wire becomes positively charged to the degree necessary to maintain its potential at the same value as that of the wall. This typically results in a linear charge density on the wire that is of order 1/2 of the beam linear charge density. Extremely strong lenses are required to properly match the beam into

and out of the zone. The rms matched radius for injection is

$$R_m = E \left(\frac{I_A}{2fI_B}\right)^{1/2} \qquad (5)$$

where E is the rms emittance, $I_A = 17\beta\gamma KA$, I_B is the beam current in KA and f is the ratio of the wire linear charge density to the beam linear charge density. R_m is typically on the order of a few millimeters. The beam radius strongly diverges upon exiting the wire zone since the rms perpendicular velocity is large,

$$\frac{v_\perp}{c} = \left(\frac{2fI_B}{I_A}\right)^{1/2} . \qquad (6)$$

The wire very strongly phase mixes electron orbits because of its highly anharmonic potential so its use is expected to symmetrize the beam in ATA.

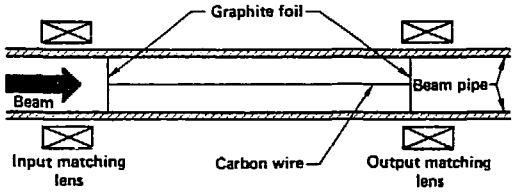

Fig. 12. Schematic of wire damping zone showing wire, supporting end foils and input and output matching magnets.

References

[1] T. J. Fessenden, W. L. Atchison, D. L. Birx, J. C. Clark, E. G. Cook, R. E. Hester, L. L. Reginato, D. Rogers Jr., R. E. Spoerlein, K. W. Struve, and T. T. Yokota, I.E.E.E. Trans. Nuc. Sci. NS-28, No. 3, 1981.

[2] T. J. Fessenden, B. W. Stallard, G. G. Berg, Rev. Sci. Inst. 43 No. 12, 1789, 1972.

[3] G. J. Caporaso, A. G. Cole, K. W. Struve, I.E.E.E. Trans. Nuc. Sci. NS-30, No. 4, 2507, 1983.

[4] V. K. Neil, L. S. Hall, R. K. Cooper, Part. Accel. 9, 213, 1979.

[5] R. J. Briggs, D. L. Birx, G. J. Caporaso, T. J. Fessenden, R. E. Hester, R. Melendez, V. K. Neil, A. C. Paul, and K. W. Struve, I.E.E.E. Trans. Nuc. Sci. NS-28, No. 3, 1981.

[6] D. S. Prono, G. J. Caporaso, A. G. Cole, R. J. Briggs, Y. P. Chong, J. C. Clark, R. W. Hester, E. J. Lauer, R. L. Spoerlein, K. W. Struve, Phys. Rev. Lett. 51, No. 9, 723, (1983).